

Article

Investigating the Relationship between Growth Rate, Shell Morphology, and Trace Element Composition of the Pacific Littleneck Clam (*Leukoma staminea*): Implications for Paleoclimate Reconstructions

Hannah L. Kempf , David A. Gold  and Sandra J. Carlson

Department of Earth and Planetary Sciences, University of California, Davis, CA 95616, USA; dgold@ucdavis.edu (D.A.G.); sjcarlson@ucdavis.edu (S.J.C.)

* Correspondence: hlkempf@ucdavis.edu

Abstract: Due to their robust preservation and widespread nature, marine bivalve shells are increasingly used as informative, high-resolution records of past environmental conditions. Unfortunately, few studies have investigated variability amongst individuals in a genetic cohort and throughout their ontogeny. We measured several morphological properties and the element patterning of 200-day-old juvenile *Leukoma staminea* (Conrad, 1837) grown in identical conditions from the same reproductive cohort. We hypothesized that slower shell growth would correspond to the reduced incorporation of trace/minor elements (Sr, Mg, and S) in the aragonite lattice, as has been documented in other biomineralizing marine invertebrates. Microprobe analyses of adult shells revealed higher levels of S, Sr, and Mg in the dark, slower-growing growth lines compared to the light, faster-growing increments, particularly in the inner shell layer, thus refuting our hypothesis. Moreover, elemental count variation within single adult shells generally tracked changes in shell microstructure (i.e., higher counts in prismatic microstructures) and growth line patterns, and these differences are detectable on a micrometer scale. Juvenile shells of different sizes showed variation in S, Sr, and Mg counts as well, but it was unclear whether the variability closely tracked changes in microstructure, body size, and/or growth line patterns. In all individuals, regardless of life stage, the outermost shell layer showed higher Sr and S count values, and these elements closely mirrored each other within individual shells. The results presented herein represent the first in-depth description of the shell mineralogy, microstructure, body size variability, and geochemical properties of modern *L. staminea*, a common eastern Pacific, shallow, infaunal bivalve, allowing for the rigorous evaluation of *L. staminea* shells as recorders of past environmental and biological change. Significant intraspecific variation in the young body size, growth band patterning, and elemental composition of individuals of the same age and genetic stock complicates the use of size alone as a proxy for age in historical studies. Additionally, elemental composition shifted from high to low values (for example, Sr ranging from ~190 to 100 counts) at a very fine (micrometer) scale within single shells, as evidenced by visible correlations between microstructure and elemental composition. While young *L. staminea* shells are likely not useful as archives of (paleo)environmental conditions, adult *L. staminea* shells are likely suitable if micrometer-scale variability in shell structure and chemistry is accounted for.



Citation: Kempf, H.L.; Gold, D.A.; Carlson, S.J. Investigating the Relationship between Growth Rate, Shell Morphology, and Trace Element Composition of the Pacific Littleneck Clam (*Leukoma staminea*): Implications for Paleoclimate Reconstructions. *Minerals* **2023**, *13*, 814. <https://doi.org/10.3390/min13060814>

Academic Editors: Chiara Lombardi, Paul D. Taylor and Frédéric Marin

Received: 8 May 2023

Revised: 10 June 2023

Accepted: 12 June 2023

Published: 14 June 2023



Copyright: © 2023 by the authors. Licensee MDPI, Basel, Switzerland. This article is an open access article distributed under the terms and conditions of the Creative Commons Attribution (CC BY) license (<https://creativecommons.org/licenses/by/4.0/>).

Keywords: biomineralization; paleoclimate; microstructure

1. Introduction

Readily preserved in a wide range of conditions due to their hard, mineralized calcium carbonate shells, bivalve molluscs are increasingly used as high-resolution records of both distant and recent past oceanographic conditions [1–4]. Despite a growing body of knowledge, few studies have investigated variability amongst individuals in a genetic cohort. To test the influence of growth rate on aragonitic biomineralization, we investigated

the shell morphology, microstructure and chemical composition of Pacific littleneck clams, *Leukoma staminea* (Conrad, 1837), of multiple sizes and life stages. We hypothesized that periods of slower growth correspond to lower values of trace/minor elements (Sr, Mg, and S) in the shell because slower calcification can allow for the exclusion of “impurities” from the CaCO₃ crystal lattice [5–7]. Interestingly, though, as calcification rate increases in *Arctica islandica* (Linnaeus, 1767), another marine bivalve, the Ba, Mg, and Sr/Ca ratios decrease in a nonlinear fashion, and patterns vary across individuals studied and locations of collection [5]. This highlights the need to study species-specific relationships between growth and trace/minor element shell chemistry. To test our hypothesis, we evaluated various morphological properties and element patterning of 200-day-old juvenile *L. staminea* clams grown in identical conditions from the same reproductive cohort. Additionally, we analyzed the parent individuals from Bodega Bay, CA to make comparisons across life stages of individuals from a common genetic stock. We then used this information to rigorously evaluate the utility of *L. staminea* shells as records of historical environments. By examining animals from multiple life stages, we captured both pre-sexual maturity and post-sexual maturity shell features and made comparisons among and within individuals. We provide the first in-depth description of the shell mineralogy, microstructure, body size variability, and geochemical properties of *L. staminea*, and we determine whether and how differences in growth rate and life stage correspond to changes in shell structure and trace element patterns.

Bivalve shell morphology, body size variability, and chemistry have been analyzed to infer historical patterns of shellfish harvesting by humans [6–8], as well as recent and paleo-oceanographic conditions [1–4]. To use shells as records of environmental and climatic trends, biominerals and the complex interplay between physiology and the environment from which they arise must be understood. Biomineralized calcite and aragonite from corals [9], foraminifera [10–12], and marine bivalves [1,13,14] can serve as records of past oceanographic conditions when evaluated with stable isotopes, and trace and/or minor elements. These organisms actively incorporate molecules present in seawater into their shells and skeletons and therefore can capture the chemical properties of seawater and record changes throughout their development. Some trace and minor elements, including Sr, Mg, Na, B, and Ba, can record properties such as seawater temperature and salinity at the time of calcification [10,14,15]. However, how element concentrations in the shell change as body size increases and shell shape changes is not always straightforward and is complicated by ontogeny, “vital” or other biological effects, and environmental conditions [15–17].

During abiotic crystallization, Sr ions can be incorporated into the aragonite lattice at concentrations approaching twice as high as in calcite due to (1) the structure of the crystal lattice and the larger size of the Sr ion and (2) because Sr is strongly precipitation-rate-dependent in inorganic calcite (but not aragonite), with slower growth leading to less incorporation [18,19]. Furthermore, inorganic aragonite shows an inverse relationship between temperature and Sr concentration [18] and is independent of precipitation rate [20]. Although metal-Ca ratios show predictable correlations with temperature in inorganic aragonite and calcite [18,20,21], the relationships show little consistency across biomineralized species and often deviate from elemental equilibrium due to several co-varying “vital effects” [22–24]. During biomineralization, vital effects, including metabolic rate, ontogenetic age, genetic variability, and growth rate, are known to affect the incorporation of elemental impurities into shells, causing discrepancies across (and within) species [23–25]. Differences in species-specific organism development may translate to some species having more dramatic vital effects than others, and some are likely more influenced by their ambient chemical environment than others. Because of these complexities, studies investigating these relationships are necessary to further document species’ variability.

Across bivalve species, immense variability in shell trace element incorporation exists. For example, the middle layer of the aragonitic venerid clam *Mercenaria campechiensis* (Gmelin, 1791) exhibits Sr/Ca ratios negatively correlated with seawater temperature [26],

while the outer layer of another venerid, *Saxidomus gigantea* (Deshayes, 1839), exhibits Sr/Ca ratios positively correlated to temperature [27]. Additionally, metal-Ca ratios can vary significantly throughout the ontogeny of a single individual, as was demonstrated in the large Mediterranean clam, *Pinna nobilis* (Linnaeus, 1758), which is a member of the more distantly related Pteriomorpha [28,29]. Such variation throughout ontogeny can impact metal-Ca ratios among individuals within a population. For example, slower-growing *Arctica islandica* individuals maintained lower Mg- and Sr-to-Ca ratios in their aragonitic shells than faster growing individuals of the same population, complicating its use as a species-specific paleo-archive and illustrating the importance of incorporating intraspecific growth rate variation into sclerochronological analyses [25]. Given these complexities, paleoclimate reconstruction using chemical proxies of biogenic materials requires a deep understanding of biomineralization mechanisms across species, among populations, and within single individuals.

In addition to chemical proxies, microstructural changes within a shell may reflect organisms' response to shifts in environment throughout development [30]. Like trace elements, though, the precise relationships between microstructure and environment are underexplored, potentially species-specific, and could vary within populations due to genetic variability. During biomineralization, the molecules needed to produce CaCO₃ microstructures are transported into and out of the calcifying fluid from the ambient environment via potentially energetically costly transport processes [31,32]. The degree to which the site of calcification is isolated from the environment varies by species [15], and the mechanisms underlying element partitioning in shells are complex and variable. In bivalve molluscs, biomineralization occurs extracellularly on organic templates, the diverse array of which are hypothesized to determine the species-specific mineralogy and shell microstructure [15,33–35]. Recent work suggests minor elements, such as Mg⁺², play an important role in the transformation of the amorphous calcium carbonate precursor to organized calcite and aragonite crystals [36,37]. Furthermore, despite the small amounts of proteinaceous material in bivalve shells, researchers have documented a diverse array of amino acid compositions across species as well as within-single species' microstructurally distinct layers [33,38], supporting the hypothesis that microstructural changes within a shell may reflect changes in organic composition at the site of calcification throughout development [35]. Clearly, both the final shell microstructure and trace/minor element geochemistry result from a complex interplay of whole-organism biological and environmental processes. While a thorough understanding of shell microstructure, growth patterning, and geochemistry is not always straightforward, it is necessary to (1) understand the mechanisms involved in element partitioning in biogenic minerals; (2) characterize the variability among individuals, conspecific populations, and among species; and (3) accurately interpret shells of marine organisms as archives of historical conditions.

Leukoma Staminea as a Study Organism

The Pacific littleneck clam, *L. staminea*, is an excellent focal species because it is geographically widespread, abundant, easily collected, and ecologically and culturally significant [39–42]. *L. staminea* is an infaunal marine bivalve (Veneridae) that burrows 5–15 cm beneath the sediment surface and is found along nearly the entire coast of western North America, ranging from Baja California, Mexico to Alaska [39,43]. Found in a variety of habitats ranging from exposed rocky beaches to low-energy mudflats, *L. staminea* is a suspension feeder that feeds on a variety of plankton [39]. Sexual maturity occurs at around 2–3 years, and spawning takes place in late-spring and early summer [39,44]. *L. staminea* have been harvested for millennia by Indigenous peoples across the northeastern Pacific coast [40,41] and remain commonly collected and eaten today. Recent research has documented *L. staminea* population decline in some areas, likely due to competition with invasive species [45].

L. staminea produces aragonitic shells that contain light and dark banding patterns in the outer layers [39,46] (Figures 1 and 2). Until this study, the fine-scale shell structure,

growth patterning, relationship between dark/light patterns and chemical properties of the shell, and patterns of ontogenetic variation in individual size and shape had not been studied extensively [46]. Generally, though, under reflected light, bivalve shell sections often exhibit patterns of light and dark banding, where light increments correspond to fast growth in optimal conditions, and dark bands to slow (or nearly ceased) growth in stressful conditions [4,47–49]. The well-studied, long-lived bivalve species *A. islandica* documents high resolution environmental trends via daily and annual growth lines that closely follow differences in shell stable isotope and elemental chemistry [2,14,50]. While the extensive research on *A. islandica* demonstrates its utility as a record of past climate and seasonal trends, research on additional bivalve species (particularly common, temperate zone species) aimed at evaluating their utility as a record of environmental change is limited [4].

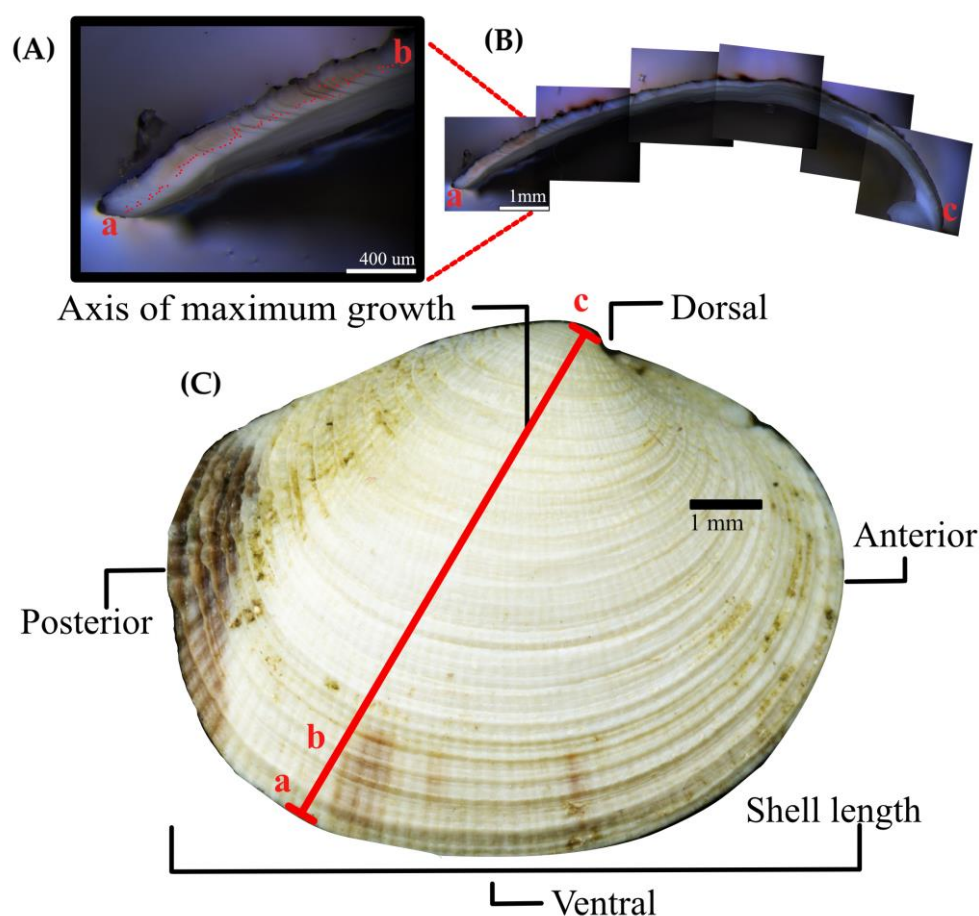


Figure 1. *L. staminea* anatomy. (A) ventral margin of juvenile; red dots within the cross section mark sub-annual growth bands; scale = 400 μm. (B) entire cross sectional view of juvenile shell; scale = 1 mm. (C) Whole-shell image and shell cross section are from a 200-day-old juvenile. Red line denotes the axis of maximum growth along the shell; scale = 1 mm.

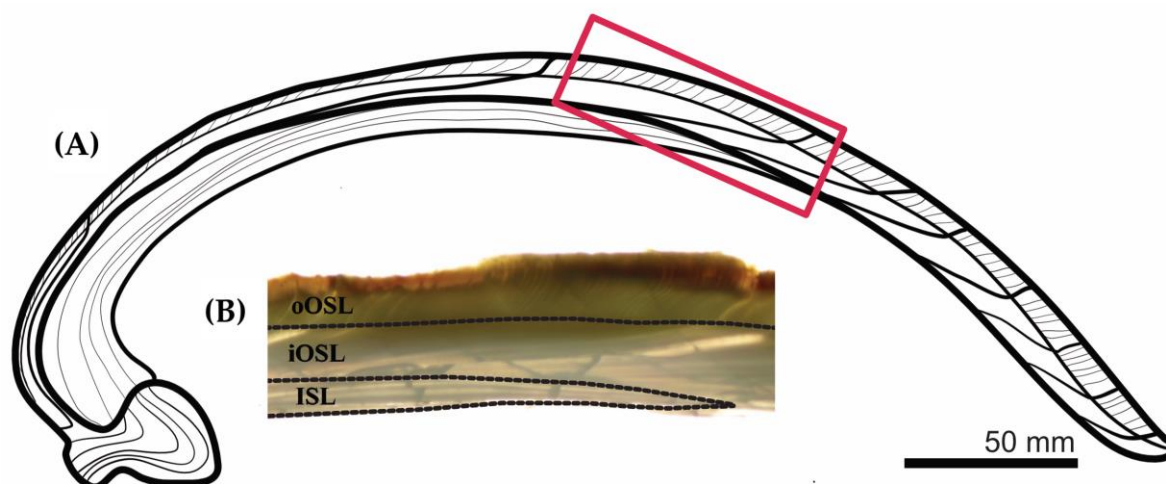


Figure 2. (A) Drawing of an *L. staminea* shell cross section showing microstructurally distinct layers. Red box denotes approximate area of the shell imaged in below in 2B. Scale: 50 mm. (B) Transmitted light microscopy image showing microstructurally distinct shell sublayers in an adult *L. staminea* shell. Scale: 50 mm.

2. Materials and Methods

2.1. Oceanographic Setting of Broodstock Sampling Location

Bodega Bay is located approximately 60 miles north of San Francisco on the central coast of California. The area sits within the California Current System, which is composed of various currents that create the complex mosaic of oceanographic conditions off the California coast [51,52]. Coastal waters around Bodega Bay experience seasonal upwelling during the spring-early summer months associated with strong alongshore winds and Ekman transport, with temperatures from ~10 to 12 °C, followed by autumn relaxation periods with temperatures around ~13 to 15 °C, and wet, moderate winters with seawater temperatures ~11 °C [53,54]. Average seawater pH varies widely from ~7.6 to ~8.0 throughout the region due to seasonally influenced physical processes, including wind stress and upwelling, which lower pH, as well as diel cycles of photosynthesis and respiration [54–57].

2.2. Sample Collection and Preparation

We analyzed a total of 41 *L. staminea* specimens, including 36 juvenile clams (ranging from ~5 mm–12 mm) and five broodstock adults (~3 cm). Adult broodstock were collected from Bodega Harbor in Bodega Bay, CA in the winter of 2021. Adults underwent a controlled mass spawn in the laboratory, which produced the juveniles used in this study (Supplemental Information). All juvenile specimens were kept in identical, consistent conditions for 200 days before they were collected from group culture in November 2021. Due to the fragility of the juvenile shells, these samples were immediately frozen in –80 °C and allowed to thaw to open the valves. Adult individuals were carefully opened using a shucking knife. Shells were cleaned by gently scraping out the soft tissues, which were then frozen in –80 °C, subsequently rinsed in water-free ethyl alcohol, and air-dried.

2.3. Shell Morphology and Growth Banding

Shell morphology was examined to identify the precise relationships between juvenile body size, growth rate, shell chemistry, and structure. Morphological characteristics measured included shell length, the length of axis of maximum growth, shell mass, and the number of internal dark growth lines visible in the entire shell (Figure 1). The whole valve shell length and axis of maximum growth of each individual was measured using digital calipers (0.1 mm accuracy), and shell mass (g) was measured using a Mettler Toledo M140E scale (Mettler-Toledo, LLC, Columbus, OH, USA) (0.0001 g).

To quantify growth banding patterns in juveniles of the same age from a genetic cohort, 18 juvenile shell cross sections were prepared and imaged using light and stereoscopic microscopes to count growth lines. The fragility of the juvenile shells made it infeasible to produce high quality polished thin sections. Therefore, juveniles were embedded in 1-inch epoxy rounds, cut in half, polished, and imaged using an Olympus SZX10 stereoscope (Olympus Corporation, Tokyo, Japan) with PRECiV software. Growth lines were counted manually on images in Affinity Designer 2 (Figure 1; Supplemental Information).

2.4. Microstructural Properties: SEM Analyses

Scanning electron microscopy (SEM) was used to generate two-dimensional images of shell microstructural textures at a very fine scale in cross-section. To document the shell microstructure and crystal orientation of each shell layer and throughout ontogeny, two broodstock adults were examined with a high-resolution scanning electron microscope (Philips XL30 SEM) (SEMTECH Solutions, Inc., North Billerica, MA, USA). To prepare samples for SEM, shell thin sections along the axis of maximum growth were prepared by gluing whole valves to a plexiglass cube, which was then covered with a layer of epoxy resin and dried overnight. A low speed Buehler Isomet saw was used to cut 200- μm sections along the axis of maximum growth for each valve. Sections were ground using Buehler silicon carbide papers of different grit sizes and mounted on a grinder-polisher machine. After each grinding step, the blocks were rinsed in an ultrasonic bath for two minutes and observed with transmitted light to check for the quality of the polish. For SEM, sections were etched in 1 vol% HCl for 10 s and bleached in 6 vol% NaOCl for 30 min. After air-drying for at least 24 h, samples were attached to SEM stubs using double-sided tape and coated with gold using a sputter coater. To identify ontogenetic variability in microstructural fabrics, micrographs were taken at or near the thickest part of the shell to capture the microstructural properties of all mineralogical layers, as well as within both growth lines and increments in two broodstock adults. Images were taken at the same sections of the shell as the electron microprobe (EMP) analyses described below and ranged from 65 \times to 2500 \times magnification.

2.5. Trace Element Composition: EMP Analyses

EMP is a non-destructive method to evaluate fine-scale element patterns in solid materials, where samples are bombarded with a condensed electron beam, which then produces X-rays characteristic of an element. To identify the precise relationships between body size; growth rate; shell structure; and the incorporation of Mg, Sr, and S, we produced two dimensional elemental maps using a JEOL JXA-8230 electron microprobe (JEOL Ltd., Tokyo, Japan) at the Stanford University Mineral and Microchemical Analysis Facility. We produced maps of S, Sr, and Mg for four individuals (one ~35 mm adult, and three juveniles ranging from 5–12 mm in length). We imaged the entire cross section for each juvenile shell and produced maps showing the section of interest in the adult shell, capturing all of the shell sublayers (Figure 2).

EMP maps were produced using wavelength-dispersive spectroscopy for high precision, highly sensitive elemental mapping at 2- μm resolution. The electron beam was regulated at a current of 400 nA with a dwell time in 100 ms in all samples. X-rays are generated at the main element peak (element k-alpha) when the shell is bombarded by electrons. Each map illustrates the relative intensity of X-ray counts along the cross section of the shell, which are reflected by a color scale indicative of the relative amount of each element (see Section 3). Beam conditions were kept constant across runs, allowing us to qualitatively compare element incorporation across different samples as well as within each sample.

2.6. Statistical Analyses

Morphological variability and relationships among growth parameters in juveniles ($n = 18$) were analyzed with linear and exponential regression. All regression analyses

were performed in R (version 4.3.0). Furthermore, in addition to a qualitative analysis of microprobe count values, we utilized Fiji to calculate the minimum, maximum, mean, and standard deviation of gray-scale values (i.e., the average of the three component colors (R, B, and G)) along line profiles of the shell [58]. This analysis was performed to quantitatively confirm element variation between structurally distinct layers in adult specimens.

3. Results

3.1. Shell Morphology and Growth Banding

Adult *L. staminea* shells exhibit three microstructurally distinct aragonitic layers. This finding differs from previous studies, which only described two distinct layers [46]. Somewhat similar to well-studied *A. islandica*, *L. staminea* shells consist of an outer shell layer with two sublayers, which we refer to as the inner (iOSL) and outer-outer shell layer (oOSL) and an inner shell layer (ISL) [50] (Figure 2). Thin sections cut to a 200- μ m uniform thickness and viewed under transmitted light reveal growth banding (i.e., dark and light sections of shell) present in the outer shell sublayers (iOSL and oOSL) (Figure 2). These growth patterns demonstrate that *L. staminea* lengthens its shell via ventral margin extension of these layers. The innermost layer contains growth lines/increments that run approximately parallel to the shell surface. This layer thickens, rather than lengthens, the shell, likely after the first shell is deposited very early in ontogeny between 6–11 mm in length (see Section 3.3), thus strengthening the shell. Furthermore, the ISL tapers off near the middle of the shell (Figure 2). Viewed under a stereoscope, juvenile shells from the same reproductive cohort also exhibited layered shells but lacked a clear boundary between the oOSL and iOSL. Further, juveniles exhibited highly variable body sizes despite rearing in identical conditions (Table 1; Figure 3). In general, greater shell length and weight correlated with more visible internal growth bands in the outer shell layer, and this relationship is statistically significant ($p < 0.001$) (Figure 3).

Table 1. Shell metrics (mm) (mean \pm standard deviation) of juvenile clams raised in identical conditions.

Shell Weight (mg) (n = 36)	Shell Length (mm) (n = 36)	Axis of Maximum Growth (mm) (n = 36)	Number of Dark Growth Lines (n = 18)
121.7 \pm 151.2	10.8 \pm 3.3	9.3 \pm 2.6	91 \pm 46

3.2. Microstructural Properties: SEM Analyses

SEM micrographs reveal three microstructurally distinct layers in the shells of adult *L. staminea*. In the iOSL and oOSL, annual and semiannual growth lines and increments all exhibited homogeneous microstructures with crystals of various sizes and orientations (Figure 4). When viewed qualitatively, the oOSL showed slightly smaller crystal sizes and more distinct boundaries between dark cessation lines and adjacent increments than the iOSL (Figure 4). Growth lines are characterized by slight textural changes in the shell cross sectional surface, but the microstructure appears to remain homogenous (Figure 4). However, there is not a clear, systematic microstructural boundary observed between a growth line and an adjacent growth increment in the SEM images in the two outer shell layers (Figure 4). The ISL was dominated by increments composed of well-organized cross acicular microstructure, and growth lines running approximately parallel to the direction of growth composed of prismatic microstructures (Figure 4). The observed growth patterns of *L. staminea* mirrored other bivalve species in some ways, including the well-studied species *Arctica islandica* [25,35,47,50,59]. For example, *A. islandica* also contains an OSL with two microstructurally different sublayers (an oOSL and an iOSL) [60]. Despite similarities to *A. islandica*, it is important to note that these two genera are classified in different families, and microstructures are incredibly variable across Bivalvia, with paleontologists, or anyone studying sclerochronological patterns in bivalves, sometimes using them as discerning characters in identifying fossils [38].

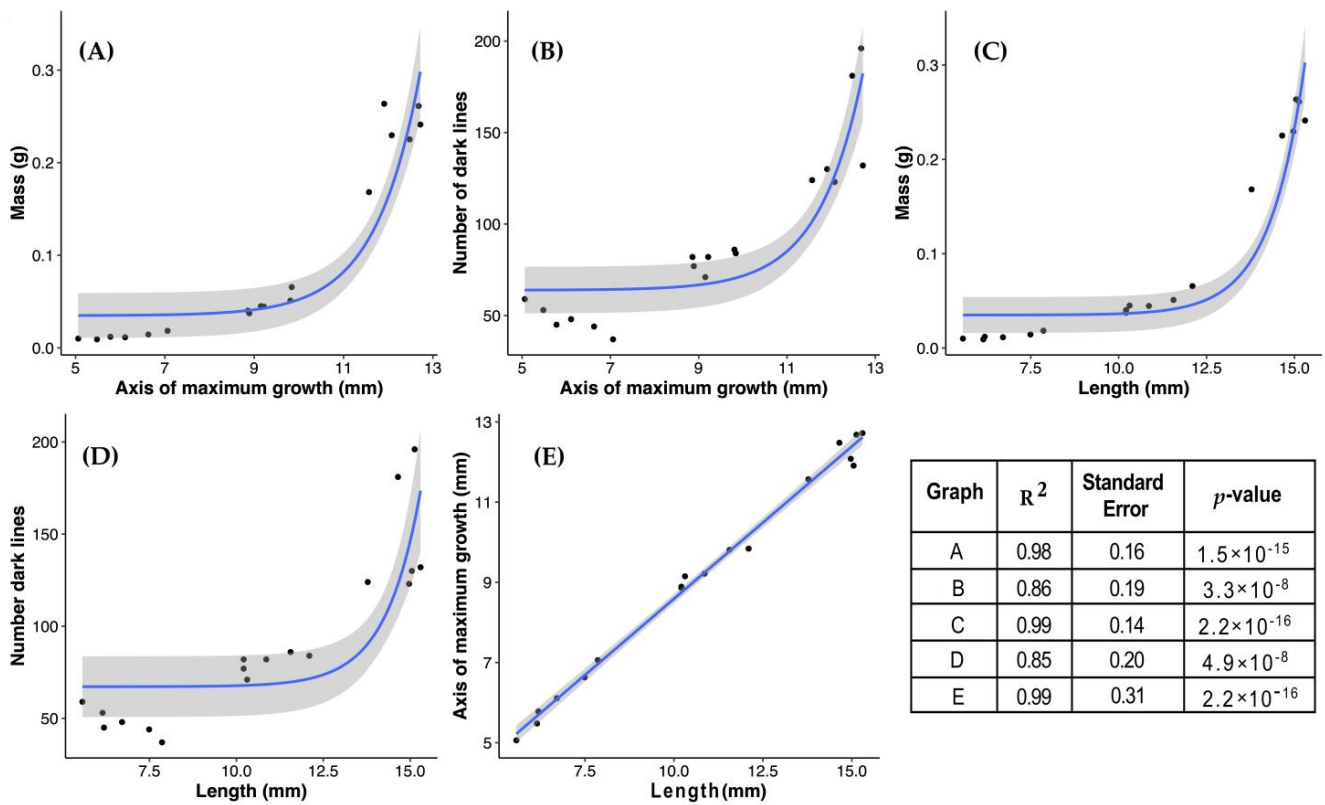


Figure 3. Morphological variability and relationships among growth parameters in juveniles (n = 18). Variables were compared using linear and exponential regression analyses in R. Data shown in (A–D) are fit with exponential regression, while (E) is a linear regression. All regression analyses were performed in R. Shaded gray shows 95% CI for regression.

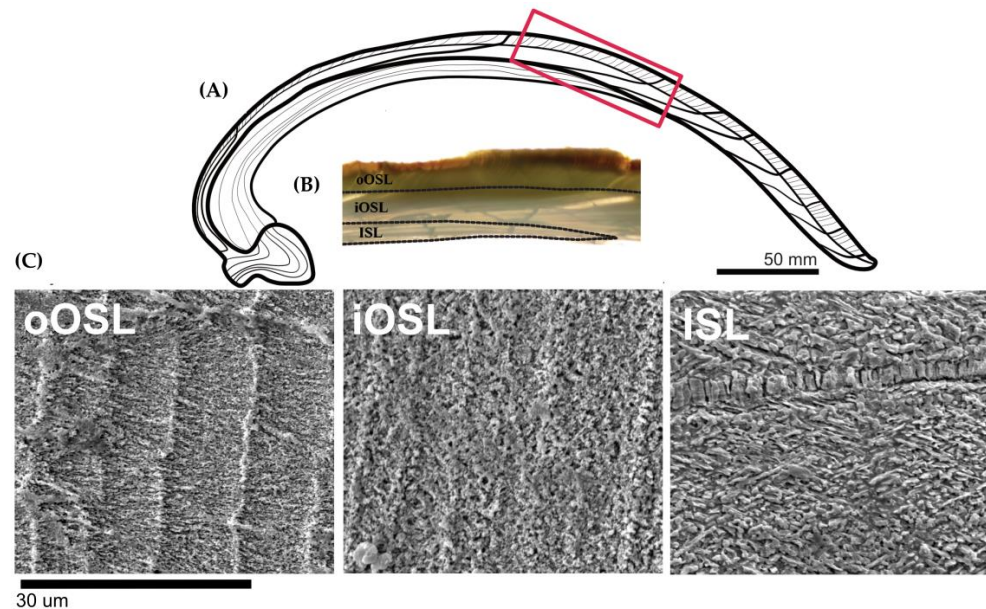


Figure 4. (A) Drawing of an *L. staminea* shell cross section showing microstructurally distinct layers, as shown in Figure 2, scale bar: 50 mm. (B) Transmitted light microscopy image showing microstructurally distinct shell sublayers in an adult *L. staminea* shell, scale bar: 50 mm. (C) SEM images of microstructures present in adult *L. staminea* shell layers; scale bar: 30 μm. oOSL = outer shell layer; ISL = inner shell layer; and iOSL = inner outer shell layer. The structure in the oOSL appears to respond more clearly to periodicities in the environment, and the ISL less clearly.

3.3. Trace Element Composition: EMP Analyses

Microprobe analyses show that Sr, S, and Mg concentrations vary throughout the shells of all analyzed shells ($n = 4$). When viewed qualitatively, all individuals clearly contain chemically distinct layers of the shell that correspond to the structurally distinct layers visible under stereoscopic and transmitted light, deposited over time during ontogeny. In the adult specimens, the area of interest captured all microstructurally distinct layers (Figure 5). The oOSL and iOSL show evidence of dark growth lines that are relatively enriched in Sr (~190 counts) and S (~50 counts) when compared to growth increments, which are distinguished by thickness (Figure 5). Growth increments, on the other hand, contain Sr values of ~100 counts and S values of ~15 counts. In the same individual, the ISL shows markedly higher Sr, with count values ranging from ~190–218. Mg varied throughout the shell in a similar manner to Sr and S, but the differences between the growth lines and increments are less distinct. Generally, Mg values ranged from ~20–40 counts throughout the entire shell section analyzed (Figure 5). Additionally, the average gray-scale values of each layer varied significantly between the ISL, iOSL, and oOSL (Figure S1; Table S1). As mentioned previously, the microstructure of the growth increments differs from that of the growth lines in the adult specimen, particularly in the inner shell layer, which corresponds closely with changes in shell elemental chemistry (Figure 6).

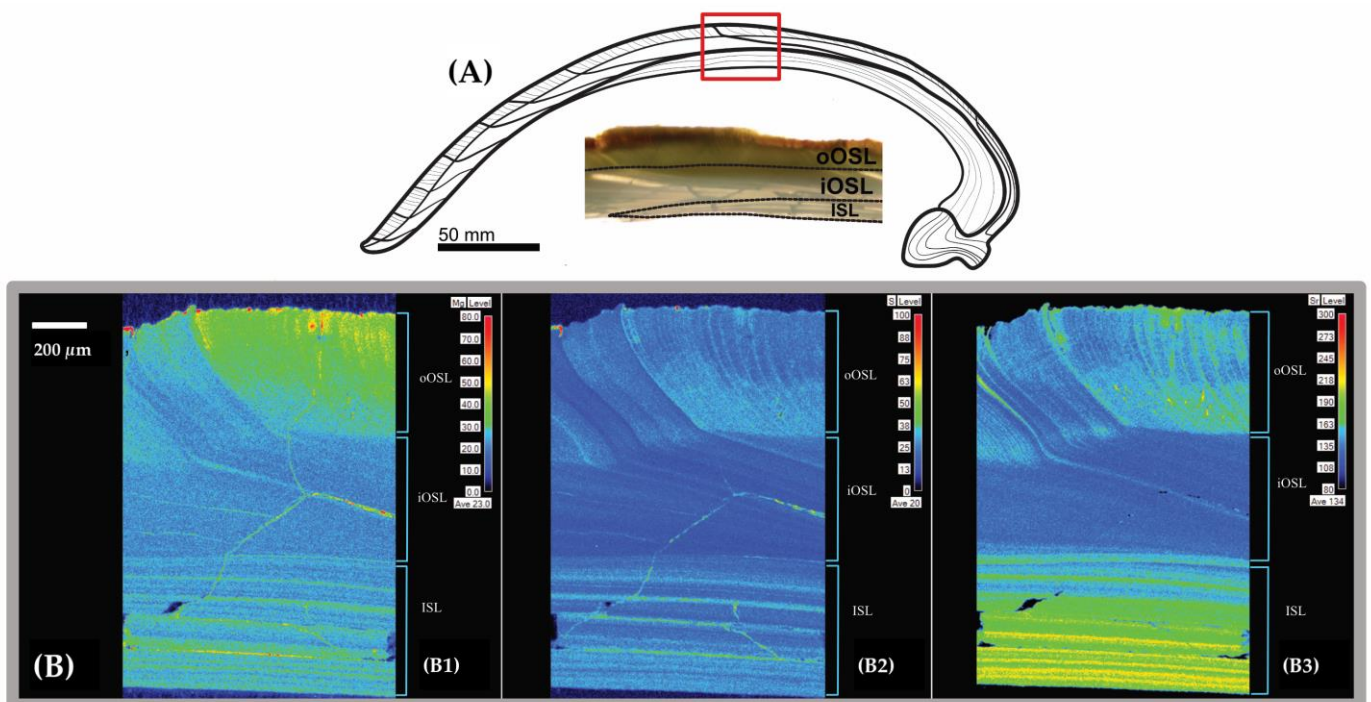


Figure 5. Element maps of adult *L. staminea*. (A) drawing of shell section and transmitted light cross sectional view of microstructurally distinct layers; red box: area of interest for element maps. (B) Element maps. B1. Mg, B2. S, B3. Sr. Scale bar: 200 μm . oOSL = outer shell layer; ISL = inner shell layer; and iOSL = inner outer shell layer.

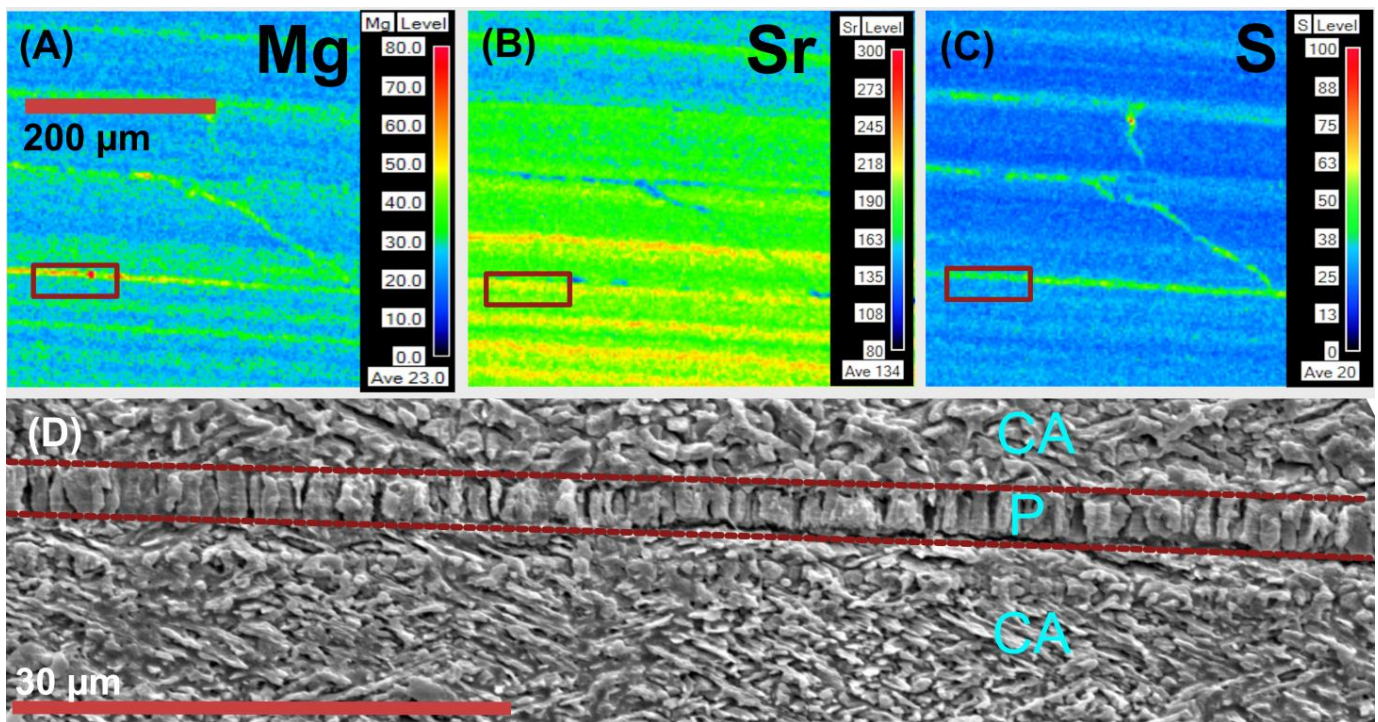


Figure 6. Inner shell layer of adult *L. staminea*. (A–C) element maps. Red boxes on maps indicate the area of interest highlighted in the SEM image. Color scales show x-ray counts from microprobe analyses. (D) SEM image in area of interest showing the correlation between microstructures and trace element counts. P = prismatic microstructure; CA = cross acicular microstructure. Dotted red line indicates boundary between growth line and growth increment in the ISL.

Juvenile shells showed variation in Sr, S, and Mg counts as well (Figure 7). In all individuals, the oOSL showed higher Sr and S values (Figure 7). In the outer layers of the juveniles, the smallest individual had the highest count values for Sr (~190 counts), followed by the largest juvenile (~170 counts) and then the medium-sized juvenile (~15 counts). For S, the smallest juvenile OSL had values ~50 counts, followed by the medium and largest juvenile, both of which had similar counts of ~42. Mg was highest in the smallest and largest juvenile OSL, with values of ~40 counts, followed by the medium juvenile, with values of ~15 counts. The medium juvenile showed little to no variation in Mg levels throughout the shell, which may be related to differences in microstructure that were not captured in this study. Interestingly, the juvenile individuals did not show clear evidence of an inner shell layer (ISL) enriched in S and Sr (Figure 7). However, we hypothesize that this pattern is observed due to the fragility of the shell and potential loss of shell material during the polishing process.

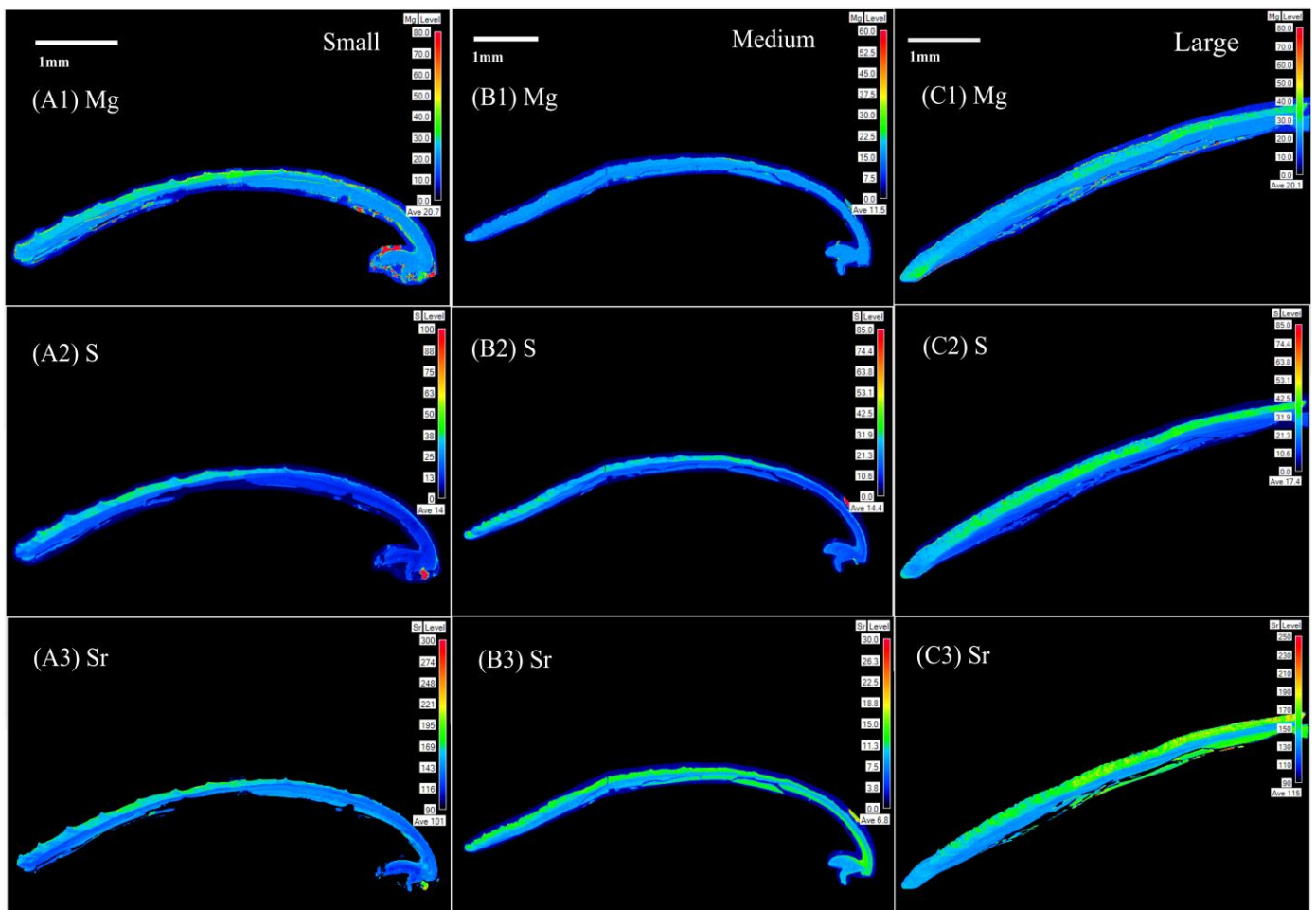


Figure 7. Microprobe analysis of juvenile *L. staminea*. (A1–A3) = small (6 mm); (B1–B3) = medium (11 mm); and (C1–C3) = large (15 mm) juvenile *L. staminea* Mg, S, and Sr values, respectively. (C1–C3) show only the ventral margin of the largest individual. Scales show relative X-ray counts for each element. Note differences in color scales between scans. EMP analyses do not allow for direct comparisons among different elemental maps. For example, if the Mg map shows more counts than the Sr map that does not indicate more Mg than Sr in the sample, i.e., Mg maps can only be compared to other Mg maps.

4. Discussion

4.1. Ontogenetic Influences on Shell Microstructure and Geochemistry

In this study, we consider the shell growth rate on two distinct temporal scales: (1) growth increments (faster and thicker) vs. growth lines (slower and thinner), and (2) early ontogeny (faster) vs. late ontogeny (slower). We hypothesized that slow shell growth would correspond to lower EMP X-ray count values of trace element incorporation in the shell, due to individuals having more time to exclude elemental “impurities” from the crystal lattice during biomineralization. Our results reject this hypothesis and suggest that the fast growth (i.e., growth increments) of aragonite in *L. staminea* leads to a depletion of Mg, Sr, and S compared to periods of slow growth (i.e., growth lines) in adult growth (Figure 5). When comparing average trace element count values of juveniles vs. adults, the outer shell layers were generally comparable. However, juveniles lacked an ISL enriched in Sr, ensuring that the average shell chemistry of the overall faster-growing juveniles contained less Mg, Sr, and S. Lastly, when comparing different sections of the adult shells, we found no detectable differences between the umbo-ward sections of the shell (earlier ontogeny, faster growth) vs. the ventral margin (most recent growth). However, the X-ray maps of the umbo and ventral margin were not complete due to irregular textures in the

shell (see Figure S2). Due to the nature of our approach, it is important to note that we did not calculate Sr/Ca ratios but instead based our results on high-resolution X-ray maps and count values, which are more qualitative in nature but allow for an extremely fine-scale investigation of element patterns. Interestingly, these results counter the previous limited work on *L. staminea* using LA-ICP-MS, which linked the faster growth rate to higher element: Ca ratios [46]. Takesue and Van Geen (2004) only analyzed the outer shell layers, which clearly document growth reduction over ontogeny as annual lines become more closely spaced [46]. However, the ISL, which they did not study, appears to be mineralized at a rate distinct from the outer layer(s), as indicated by the higher Sr levels (Figures 5 and 6). This supports the idea that different regions of the mantle mineralize at different rates and different times throughout ontogeny. We also add finer-scale images of element patterns, as well as descriptions of shell microstructure, and provide useful information on juveniles and their variability in size and growth during the same, known period, from an extant population living further south than previously studied.

EMP count values for S correlated to those for Sr, and to a lesser extent Mg in *L. staminea* shells. We suspect that this pattern is a manifestation of the organisms' modulation of insoluble and soluble organic matrices, which often contain sulfur, throughout development [35,61–66]. Interestingly, however, when comparing the life stages of our samples, not all juvenile individuals show clear evidence of an ISL enriched in S and Sr, suggesting that the trace elemental incorporation of these elements in the thickening portion of the shell may occur later in ontogeny. In our juvenile samples, inner layers relatively enriched in Sr start to form between 6–11 mm in length, but the smallest individual lacks evidence of an ISL, and it is not until the juveniles are closer to 11 mm in length that the Sr values in the ISL approach values akin to the adult ISL (Figure 7). The thick, Sr-rich ISL present in our adult samples may indicate that this inner layer grows later and more slowly than the oOSL and iOSL, which are not as enriched in Sr (Figure 5). Additionally, within Veneridae, microstructural variation between the myostracum and underlying shell in the ISL exists [67]. This warrants further investigation of the ISL to identify precise relationships between microstructure, geochemistry, and how these vary between the myostracum and the underlying shell.

Juvenile *L. staminea* showed, like the adults, clear microstructural evidence of ventral margin extension via growth lines/increments in the shells and a structurally distinct thickening inner shell when viewed under a stereoscope. While these internal growth band patterns could not be directly correlated to our microprobe data, we suspect that the microprobe resolution of 2 μm , while very fine, may have still been too coarse to detect even-finer scale patterns of elemental variation that may be present in juvenile shells. One potential reason for this observation could be that the shell crystal size was too small (sub-micrometer size). Another possibility is that the juvenile shell contained significant amounts of amorphous calcium carbonate (ACC) in its structure. Although the transformation mechanisms of ACC to crystalline material are elusive, several recent studies have investigated the role of ACC in biomineralization and documented its presence in bivalve shells using novel imaging techniques [36,68–71]. Interestingly, precipitation experiments involving inorganic calcium carbonate from seawater have shown that ACC can differ chemically quite significantly from crystalline CaCO_3 [72], which could explain the lack of clear elemental patterns in our juvenile samples.

Although we could not identify precise correlations in elemental and growth line patterns in 200-day-old individuals, juveniles exhibited notable differences in trace and minor element composition within single shells, which varied across individuals of different sizes and the same age. In the outer shell layer, the large and medium-sized (i.e., faster-growing) individuals showed the lowest count values for S (~42), while the smallest individual had only slightly higher counts of ~50. For Sr, the medium sized (moderately fast growing) individuals had the lowest count value for Sr (~15 counts), which was significantly lower than both the fastest and slowest growing individuals (190 and 170 for Sr, respectively). Growth rate differences early in ontogeny may have some relationship to the

elemental incorporation of Sr into the shell biomineral; however, the different expressions of element incorporation in juvenile *L. staminea* are perhaps a result of other physiological and/or genetic variation present within the population. In all, these results suggest that ontogenetic and microstructural biases must be considered when using *L. staminea* for paleoclimate reconstructions and proxy development, particularly if one is interested in the ISL [73].

4.2. Population-Level Variability in Growth and Studying Biomineralization through Time

The mineralized shell developed early on in mollusc evolution and was subsequently lost in some lineages, making variability in shell structure a point of interest for those studying morphological change, phylogenetic histories, heterochrony, and macroevolutionary trends through time [2,38,48,74,75]. In some studies, shell size is used as a proxy for age, and annually precipitated growth patterns can provide age-at-size information and document life history [75]. Often, researchers must distinguish annual lines from “disturbance lines,” which can occur from storms, predation attempts, and/or abnormal environmental events and are in many ways morphologically like annual lines [31]. One way that researchers distinguish these lines is via close examination of the “microincrements,” or subannual lines, which precede the darker/thicker annual lines in shells [46]. Microincrements supposedly decrease uniformly in width leading up to an annual line, while disturbance lines occur more abruptly amid regularly spaced microincrements [48].

Microincrements in bivalve shells have been empirically linked to a variety of environmental processes, including tidal cycles, nutrient availability, and dark/light cycles [48,76–85]. The production of microincrements may stem from endogenous rhythms controlled by “biological clocks” [77]. Biological clocks exist across the tree of life, ranging from cyanobacteria, to fungi, mammals, and molluscs [86–89]. These systems are composed of (1) a central molecular oscillator that tracks time; (2) environmental cues that measure time; and (3) rhythms of physiological, biochemical, or behavioral activities of an organism, such as gape (opening) patterns in marine bivalves [90,91]. Biological clocks are ultimately under genetic, rather than environmental, control and serve to optimize the energetic balance of organisms by obtaining nutrients and using energy when it is available [77]. Aschoff (1981) argued that biological clocks can be “auto-entertained,” meaning that the observed physiological oscillations can continue even if the organism is kept under constant conditions, similar to what we observed in *L. staminea* juveniles [92]. These patterns are observable, likely because the biological clock is highly conserved [93]. Biological clocks have been documented in several bivalve species, mainly at the daily and tidal frequencies, and posited as responsible for growth line/increment patterns [17,77,84]. Further, in recent years, homologous clock genes have been studied in the mussels *Mytilus edulis* [86] and *Mytilus californianus* [94], the oyster *Magallana gigas* [95], and the scallops *Argopecten irradians* [96] and *Chlamys islandica* [97].

Interestingly, though, microincrements within the juvenile shells of *L. staminea* did not present in a regular, predictable pattern but occurred somewhat haphazardly throughout all the analyzed individuals (Figure S3). This also occurs in many oysters, making them a less common study group in sclerochronology studies [98,99]. Variability in the observed gross morphology and growth banding patterns may reflect inherent intrapopulation genetic variability present in the sample. Additionally, distinct environmental drivers of the biological clock system beyond those classically studied (i.e., photoperiod and/or temperature), such as food availability, should be considered and further evaluated and may shed light on *L. staminea* growth banding. It is likely that size variability within the juvenile cohort corresponds to variability in their feeding habits (i.e., larger individuals may have been feeding more and therefore may have produced larger shells with more growth lines/increments). While we did not measure feeding rate in our juvenile samples, further studies in controlled laboratory studies should investigate the role of food availability/consumption on shell growth patterning.

Marine bivalves, including *L. staminea*, typically decrease their shell growth rate throughout ontogeny, and species-specific ontogenetic patterns can affect the duration

and timing of the growing season (i.e., when increments are formed vs. when lines are formed) [100–102]. We suspect this may also vary within species with large geographic ranges, such as *L. staminea*, where local adaptation and population genetic variation can occur. Additionally, how the variability in growth rate, growth banding, and elemental composition observed in our young, juvenile population grown in the lab would scale throughout their ontogeny is unknown and warrants further study. To better understand these questions, more data on adult populations of the same, known age, and location are necessary. Lastly, a deeper investigation into the genetic mechanisms of the biological clock in *L. staminea* and the role of the feeding rate could yield important information regarding the timing and tempo of their growth line and trace and minor element incorporation patterns.

4.3. Potential of *L. staminea* to Document (Paleo)Environmental Conditions

As biomineralization mechanisms vary both across and within species, we argue that both morphological and geochemical measurements must be leveraged to accurately use bivalve shells as a record of paleoenvironmental conditions, growth rate, and/or lifespan [103]. In addition to trace elements, the stable oxygen isotope composition of bivalve shell carbonate, which typically varies along the axis of maximum growth, can and should be used since it is highly temperature-dependent [23,104] and therefore responds to seasonal trends in temperature. Oxygen isotopes, when coupled with clear growth band patterns, can thus reveal chronological environmental information from the shell. Early research demonstrated that the oxygen isotope composition of bivalve shell carbonate is precipitated at, or near, isotopic equilibrium with the seawater in which the organism builds its shell and therefore reflects the oxygen-isotope composition of the seawater ($\delta^{18}\text{O}_w$) and ambient temperature [104]. Since then, $\delta^{18}\text{O}$ of both aragonitic and calcitic bivalve shells has been used as a record of past seawater temperatures [3,105–109]. However, kinetic effects during biomineralization can cause species-specific deviations from isotopic equilibrium [100,109–111]. Owen et al. (2002) documented a relationship between low shell growth rate and shell $\delta^{18}\text{O}$ that was more positive (differing by $\sim 0.4\%$, corresponding to an offset of $1.9\text{ }^\circ\text{C}$) than the predicted values of inorganic calcite in isotopic equilibrium with seawater [100]. Additionally, Cusack et al. (2008) found significant differences in isotopic composition (differing by $\sim 0.4\%$), depending on whether the outer prismatic or inner nacreous section of the shell was sampled, similar to our results with Sr incorporation differences between the inner and outer shell layers [33]. As is the case with trace/minor elements, we suspect ontogenetic and population-level variability in growth rate and other physiological properties may also obscure recorded isotope values.

Because elemental composition changed significantly at the very fine (micrometer) scale within single shells in our study, as evidenced by visible correlations between microstructure and elemental composition, we argue that adult *L. staminea* shells are only suitable for further proxy-development if micrometer-scale variability in the shell structure and chemistry is accounted for to minimize time-averaging. To do so, researchers should use both electron microprobe mapping tools, SEM, and quantitative analyses such as fine-scale LA-ICP-MS or stable isotope sampling. Although previous work documented in situ trace element measurements of Sr and Mg in the outer shell layer of *L. staminea* [46], these results were based on samples ablated from 90–100 μm diameter spots, which comprise an overly coarse resolution to accurately capture the elemental variability present in the shell. LA-ICP-MS typically requires the sampling of at least $\sim 50\text{ }\mu\text{m}$ spot size [112], but new high-resolution LA-ICP-MS technologies allow for elemental analysis at $\sim 10\text{ }\mu\text{m}$ resolution [113]. Additionally, correlations between crystal microstructure and elemental chemistry in adult specimens point to the need for the detailed mapping of the crystal fabrics in addition to analyses of stable isotopes and/or trace elements, due to the close relationships among them [60,114]. These various shell characteristics must be accounted for and necessitate the rigorous evaluation of modern, local populations prior to (paleo)environmental analyses. In all, our results highlight the biological influences underlying the shell charac-

teristics of *L. staminea*, demonstrating the importance of accounting for both ontogenetic and population-level variability. These issues likely affect species other than *L. staminea* and are particularly problematic for extinct species. In all, the best way forward for (paleo)environmental reconstructions using *L. staminea*, or any aragonitic bivalve, is to take a multi-proxy approach drawing upon morphological and geochemical properties, and account for micrometer-scale variability that occurs throughout the organism's lifespan.

5. Conclusions

We provide the first detailed description of shell mineralogy, microstructure, body size variability, and geochemical properties of modern *L. staminea*. We measured various morphological properties and element patterning of 200-day-old juveniles grown in identical conditions from the same reproductive cohort, as well as their parent individuals.

5.1. Morphology and Growth Rate

We hypothesized that slow shell growth yields lower trace/minor element incorporation in the shell, due to individuals having more time to exclude elemental "impurities" from the biomineral. Our results refute our hypothesis. In adults, growth increments (fast growth) were relatively depleted in Mg, Sr, and S compared to growth lines (i.e., slow growth) (Figure 5). When comparing different ontogenetic sections of the adult shells, we found no detectable differences in count values between the umbo (earlier ontogeny, faster growth), the middle, and the ventral margin (most recent growth). However, microprobe maps of the umbo and ventral margin were not complete due to irregular textures in the shell, thus warranting further examination.

5.2. Microstructure and Trace Elements

Growth lines and increments showed distinct microstructural and geochemical properties. Microprobe analyses revealed higher levels of S, Sr, and Mg in the prismatic growth lines, particularly in the inner shell layer, suggesting a link between microstructure and trace element chemistry. Further, we provide the first structural and geochemical description of the inner shell layer, which appears to mineralize at a slower rate than the outer layers and only once the shell length reaches between ~6–11 mm, demonstrating that different regions of the mantle mineralize at distinct rates and times throughout ontogeny. While juvenile shells of different sizes also showed variation in S, Sr, and Mg, we could not link elemental patterns clearly to microstructure, body size, and/or growth line patterns. Significant intraspecific variation in the body size, growth band patterning, and elemental composition of individuals of the same age and genetic stock nevertheless complicates the use of size as a proxy for age in historical studies. Juvenile *L. staminea* shells are likely not useful for paleontological and/or (paleo)environmental research due to these issues as well as to potential diagenetic alteration. Lastly, because elemental composition changed significantly at the micrometer scale within single shells, we argue that *L. staminea* shells are only suitable if micrometer-scale variability in the shell structure and chemistry is accounted for to minimize time-averaging and if a multi-proxy approach to environmental reconstruction is adopted. Further studies examining the role of the biological clock and vital effects on biomineralization, and how these processes vary throughout ontogeny and across populations, are warranted to further rigorously evaluate the utility of *L. staminea*, and other bivalve species, in paleoenvironmental studies.

Supplementary Materials: The following supporting information can be downloaded at <https://www.mdpi.com/article/10.3390/min13060814/s1>, Figure S1: Line profiles for gray-scale variance; Figure S2: Irregular textures in adult shell; Figure S3: Haphazard expression of growth banding within a single juvenile shell; and Table S1: Mean, standard deviation, maximum, and minimum gray-scale values.

Author Contributions: Conceptualization, H.L.K. and S.J.C.; methodology, H.L.K. and S.J.C.; formal analysis, H.L.K.; investigation, H.L.K.; resources, H.L.K., S.J.C. and D.A.G.; data curation, H.L.K.; writing—original draft preparation, H.L.K.; writing—review and editing, H.L.K., S.J.C. and D.A.G.; visualization, H.L.K.; supervision, H.L.K., S.J.C. and D.A.G.; and funding acquisition, H.L.K. and D.A.G. All authors have read and agreed to the published version of the manuscript.

Funding: This research was supported by a California Sea Grant Graduate Research Fellowship (Grant NA22OAR4170106) to H.L.K.

Data Availability Statement: The data presented in this study are available in the Supplementary Materials. Unprocessed data are available upon request from the authors.

Acknowledgments: Thank you to Joe Newman and the Bodega Marine Lab Aquatic Resources Group for their help developing a spawn protocol for *L. staminea*. All the thin sections and epoxy rounds were prepared by Greg Baxter. Thank you to Sarah Roeske for helping us interpret our microprobe data.

Conflicts of Interest: The authors declare no conflict of interest. The funders had no role in the design of the study; in the collection, analyses, or interpretation of data; in the writing of the manuscript; or in the decision to publish the results.

References

- Schöne, B.R.; Pfeiffer, M.; Pohlmann, T.; Siegismund, F. A Seasonally Resolved Bottom-Water Temperature Record for the Period AD 1866–2002 Based on Shells of *Arctica Islandica* (Mollusca, North Sea). *Int. J. Climatol.* **2005**, *25*, 947–962. [\[CrossRef\]](#)
- Schöne, B.R.; Gillikin, D.P. Unraveling Environmental Histories from Skeletal Diaries—Advances in Sclerochronology. *Palaeogeogr. Palaeoclimatol. Palaeoecol.* **2013**, *373*, 1–5. [\[CrossRef\]](#)
- Trofimova, T.; Andersson, C.; Bonitz, F.G.W.; Pedersen, L.-E.R.; Schöne, B.R. Reconstructing Early Holocene Seasonal Bottom-Water Temperatures in the Northern North Sea Using Stable Oxygen Isotope Records of *Arctica Islandica* Shells. *Palaeogeogr. Palaeoclimatol. Palaeoecol.* **2021**, *567*, 110242. [\[CrossRef\]](#)
- Vriesman, V.P.; Carlson, S.J.; Hill, T.M. Investigating Controls of Shell Growth Features in a Foundation Bivalve Species: Seasonal Trends and Decadal Changes in the California Mussel. *Biogeosciences* **2022**, *19*, 329–346. [\[CrossRef\]](#)
- Cannarozzi, N.R.; Kowalewski, M. Seasonal Oyster Harvesting Recorded in a Late Archaic Period Shell Ring. *PLoS ONE* **2019**, *14*, e0224666. [\[CrossRef\]](#)
- Eerkens, J.W.; Byrd, B.F.; Spero, H.J.; Fritschi, A.K. Stable Isotope Reconstructions of Shellfish Harvesting Seasonality in an Estuarine Environment: Implications for Late Holocene San Francisco Bay Settlement Patterns. *J. Archaeol. Sci.* **2013**, *40*, 2014–2024. [\[CrossRef\]](#)
- Jenkins, J.A. Methods for Inferring Oyster Mariculture on Florida’s Gulf Coast. *J. Archaeol. Sci.* **2017**, *80*, 74–82. [\[CrossRef\]](#)
- Allison, N.; Finch, A.A. High-Resolution Sr/Ca Records in Modern *Porites Lobata* Corals: Effects of Skeletal Extension Rate and Architecture. *Geochem. Geophys. Geosys.* **2004**, *5*, 1–10. [\[CrossRef\]](#)
- Eggs, S.; De Deckker, P.; Marshall, J. Mg/Ca Variation in Planktonic Foraminifera Tests: Implications for Reconstructing Palaeo-Seawater Temperature and Habitat Migration. *Earth Planet. Sci. Lett.* **2003**, *212*, 291–306. [\[CrossRef\]](#)
- Sadekov, A.Y.; Eggs, S.M.; De Deckker, P. Characterization of Mg/Ca Distributions in Planktonic Foraminifera Species by Electron Microprobe Mapping. *Geochem. Geophys. Geosyst.* **2005**, *6*, 1–14. [\[CrossRef\]](#)
- Spero, H.J.; Lea, D.W. Experimental Determination of Stable Isotope Variability in *Globigerina Bulloides*: Implications for Paleooceanographic Reconstructions. *Mar. Micropaleontol.* **1996**, *28*, 231–246. [\[CrossRef\]](#)
- Poulain, C.; Gillikin, D.P.; Thébault, J.; Munaron, J.M.; Bohn, M.; Robert, R.; Paulet, Y.-M.; Lorrain, A. An Evaluation of Mg/Ca, Sr/Ca, and Ba/Ca Ratios as Environmental Proxies in Aragonite Bivalve Shells. *Chem. Geol.* **2015**, *396*, 42–50. [\[CrossRef\]](#)
- Schöne, B.R.; Zhang, Z.; Radermacher, P.; Thébault, J.; Jacob, D.E.; Nunn, E.V.; Maurer, A.-F. Sr/Ca and Mg/Ca Ratios of Ontogenetically Old, Long-Lived Bivalve Shells (*Arctica Islandica*) and Their Function as Paleotemperature Proxies. *Palaeogeogr. Palaeoclimatol. Palaeoecol.* **2011**, *302*, 52–64. [\[CrossRef\]](#)
- Ulrich, R.N.; Guillermic, M.; Campbell, J.; Hakim, A.; Han, R.; Singh, S.; Stewart, J.D.; Román-Palacios, C.; Carroll, H.M.; De Corte, I.; et al. Patterns of Element Incorporation in Calcium Carbonate Biominerals Recapitulate Phylogeny for a Diverse Range of Marine Calcifiers. *Front. Earth Sci.* **2021**, *9*, 1–26. [\[CrossRef\]](#)
- Markulin, K.; Peharda, M.; Mertz-Kraus, R.; Schöne, B.R.; Uvanović, H.; Kovač, Ž.; Janeković, I. Trace and Minor Element Records in Aragonitic Bivalve Shells as Environmental Proxies. *Chem. Geol.* **2019**, *507*, 120–133. [\[CrossRef\]](#)
- Warter, V.; Erez, J.; Müller, W. Environmental and Physiological Controls on Daily Trace Element Incorporation in *Tridacna Crocea* from Combined Laboratory Culturing and Ultra-High Resolution LA-ICP-MS Analysis. *Palaeogeogr. Palaeoclimatol. Palaeoecol.* **2018**, *496*, 32–47. [\[CrossRef\]](#)
- Kinsman, D.J.J.; Holland, H.D. The Co-Precipitation of Cations with CaCO₃—IV. The Co-Precipitation of Sr²⁺ with Aragonite between 16° and 96 °C. *Geochim. Cosmochim. Acta* **1969**, *33*, 1–17. [\[CrossRef\]](#)

18. Tesoriero, A.J.; Pankow, J.F. Solid Solution Partitioning of Sr^{2+} , Ba^{2+} , and Cd^{2+} to Calcite. *Geochim. Cosmochim. Acta* **1996**, *60*, 1053–1063. [[CrossRef](#)]
19. Zhong, S.; Mucci, A. Calcite and Aragonite Precipitation from Seawater Solutions of Various Salinities: Precipitation Rates and Overgrowth Compositions. *Chem. Geol.* **1989**, *78*, 283–299. [[CrossRef](#)]
20. Oomori, T.; Kaneshima, H.; Maezato, Y.; Kitano, Y. Distribution Coefficient of Mg^{2+} Ions between Calcite and Solution at 10–50 °C. *Mar. Chem.* **1987**, *20*, 327–336. [[CrossRef](#)]
21. Schleinhofer, N.; Raddatz, J.; Evans, D.; Gerdes, A.; Flögel, S.; Voigt, S.; Büscher, J.V.; Wisshak, M. Compositional Variability of Mg/Ca, Sr/Ca, and Na/Ca in the Deep-Sea Bivalve *Acesta Excavata* (Fabricius, 1779). *PLoS ONE* **2021**, *16*, e0245605. [[CrossRef](#)] [[PubMed](#)]
22. Urey, H.C.; Lowenstam, H.A.; Epstein, S.; McKinney, C.R. Measurement of Paleotemperatures and Temperatures of the Upper Cretaceous of England, Denmark and the Southeastern United States. *Bull. Geol. Soc. Am.* **1951**, *62*, 399–416. [[CrossRef](#)]
23. Weiner, S.; Dove, P.M. An Overview of Biomineralization Processes and the Problem of the Vital Effect. *Rev. Mineral. Geochem.* **2003**, *54*, 1–29. [[CrossRef](#)]
24. Ballesta-Artero, I.; Zhao, L.; Milano, S.; Mertz-Kraus, R.; Schöne, B.R.; van der Meer, J.; Witbaard, R. Environmental and Biological Factors Influencing Trace Elemental and Microstructural Properties of Arctica Islandica Shells. *Sci. Total Environ.* **2018**, *645*, 913–923. [[CrossRef](#)]
25. Surge, D.; Walker, K.J. Geochemical Variation in Microstructural Shell Layers of the Southern Quahog (*Mercenaria campechiensis*): Implications for Reconstructing Seasonality. *Palaeogeogr. Palaeoclimatol. Palaeoecol.* **2006**, *237*, 182–190. [[CrossRef](#)]
26. Gillikin, D.P.; Lorrain, A.; Navez, J.; Taylor, J.W.; André, L.; Keppens, E.; Baeyens, W.; Dehairs, F. Strong Biological Controls on Sr/Ca Ratios in Aragonitic Marine Bivalve Shells. *Geochem. Geophys. Geosyst.* **2005**, *6*, 1–16. [[CrossRef](#)]
27. Freitas, P.S.; Clarke, L.J.; Kennedy, H.; Richardson, C.A.; Abrantes, F. Environmental and Biological Controls on Elemental (Mg/Ca, Sr/Ca and Mn/Ca) Ratios in Shells of the King Scallop *Pecten Maximus*. *Geochim. Cosmochim. Acta* **2006**, *70*, 5119–5133. [[CrossRef](#)]
28. Richardson, C.A.; Peharda, M.; Kennedy, H.; Kennedy, P.; Onofri, V. Age, Growth Rate and Season of Recruitment of *Pinna Nobilis* (L) in the Croatian Adriatic Determined from Mg:Ca and Sr:Ca Shell Profiles. *J. Exp. Mar. Biol. Ecol.* **2004**, *299*, 1–16. [[CrossRef](#)]
29. Milano, S.; Schöne, B.R.; Witbaard, R. Changes of Shell Microstructural Characteristics of *Cerastoderma edule* (Bivalvia)—A Novel Proxy for Water Temperature. *New Res. Methods Appl. Sclerochronol.* **2017**, *465*, 395–406. [[CrossRef](#)]
30. Clark, G.R. Growth Lines in Invertebrate Skeletons. *Annu. Rev. Earth Planet. Sci.* **1974**, *2*, 77–99. [[CrossRef](#)]
31. McConnaughey, T. Biomineralization Mechanisms. In *Origin, Evolution, and Modern Aspects of Biomineralization in Plants and Animals*; Crick, R.E., Ed.; Springer: Boston, MA, USA, 1989; pp. 57–73. [[CrossRef](#)]
32. Cusack, M.; Freer, A. Biomineralization: Elemental and Organic Influence in Carbonate Systems. *Chem. Rev.* **2008**, *108*, 4433–4454. [[CrossRef](#)]
33. Falini, G.; Albeck, S.; Weiner, S.; Addadi, L. Control of Aragonite or Calcite Polymorphism by Mollusk Shell Macromolecules. *Science* **1996**, *271*, 67–69. [[CrossRef](#)]
34. Shirai, K.; Schöne, B.R.; Miyaji, T.; Radarmacher, P.; Krause, R.A.; Tanabe, K. Assessment of the Mechanism of Elemental Incorporation into Bivalve Shells (*Arctica Islandica*) Based on Elemental Distribution at the Microstructural Scale. *Geochim. Cosmochim. Acta* **2014**, *126*, 307–320. [[CrossRef](#)]
35. Evans, D.; Gray, W.R.; Rae, J.W.B.; Greenop, R.; Webb, P.B.; Penkman, K.; Kröger, R.; Allison, N. Trace and Major Element Incorporation into Amorphous Calcium Carbonate (ACC) Precipitated from Seawater. *Geochim. Cosmochim. Acta* **2020**, *290*, 293–311. [[CrossRef](#)]
36. Mergelsberg, S.T.; De Yoreo, J.J.; Miller, Q.R.S.; Marc Michel, F.; Ulrich, R.N.; Dove, P.M. Metastable Solubility and Local Structure of Amorphous Calcium Carbonate (ACC). *Geochim. Cosmochim. Acta* **2020**, *289*, 196–206. [[CrossRef](#)]
37. Marin, F. The Formation and Mineralization of Mollusk Shell. *Front. Biosci.* **2012**, *4*, 1099–1125. [[CrossRef](#)]
38. Fraser, C.M.; Smith, G.M. Notes on the Ecology of the Little Neck Clam. *Paphia Staminea* Conrad. *Trans. R. Soc. Can. Ser.* **1928**, *3*, 249–269.
39. Lepofsky, D.; Smith, N.; Cardinal, N.; Harper, J.; Morris, M.; Elroy White, G.; Bouchard, R.; Kennedy, D.; Solomon, A.; Puckett, M.; et al. Ancient Shellfish Mariculture on the Northwest Coast of North America. *Am. Antiq.* **2015**, *80*, 236–259. [[CrossRef](#)]
40. Schneider, T.; DeAntoni, G.; Hill, A.; Apodaca, A. Indigenous Persistence and Foodways at the Toms Point Trading Post (CA-MRN-202), Tomales Bay, California. *J. Calif. Gt. Basin Anthropol.* **2018**, *38*, 51–73.
41. Smith, G.M. Food Material as a Factor in Growth Rate of Some Pacific Clams. *Trans. R. Soc. Can. Ser.* **1928**, *3*, 287–291.
42. Harrington, R.J. Skeletal Growth Histories of *Protothaca Staminea* Conrad and *Protothaca Grata* Say throughout Their Geographic Ranges Northeastern Pacific. *Veliger* **1987**, *30*, 148–158.
43. Feder, H.M.; Hendee, J.C.; Holmes, P.; Mueller, G.J.; Paul, A.J. Examination of a Reproductive Cycle of *Protothaca Staminea* Using Histology, We Weight-Dry Weight Ratios, and Condition Indices. *Veliger* **1979**, *22*, 182–187.
44. Bendell, L.I. Evidence for Declines in the Native *Leukoma Staminea* as a Result of the Intentional Introduction of the Non-Native *Venerupis philippinarum* in Coastal British Columbia, Canada. *Estuaries Coasts* **2014**, *12*, 369–380. [[CrossRef](#)]

45. Takesue, R.K.; van Geen, A. Mg/Ca, Sr/Ca, and Stable Isotopes in Modern and Holocene Protothaca Staminea Shells from a Northern California Coastal Upwelling Region. *Geochim. Cosmochim. Acta* **2004**, *68*, 3845–3861. [[CrossRef](#)]
46. Schöne, B.R.; Dunca, E.; Fiebig, J.; Pfeiffer, M. Mutvei's Solution: An Ideal Agent for Resolving Microgrowth Structures of Biogenic Carbonates. *Palaeogeogr. Palaeoclimatol. Palaeoecol.* **2005**, *228*, 149–166. [[CrossRef](#)]
47. Schöne, B.; Surge, D. *Bivalve Sclerochronology and Geochemistry*; Paleontological Institute: Moscow, Russia, 2012; pp. 1–24.
48. Strasser, C.A.; Mullineaux, L.S.; Walther, B.D. Growth Rate and Age Effects on Mya Arenaria Shell Chemistry: Implications for Biogeochemical Studies. *J. Exp. Mar. Biol. Ecol.* **2008**, *355*, 153–163. [[CrossRef](#)]
49. Schöne, B.R. Arctica Islandica (Bivalvia): A Unique Paleoenvironmental Archive of the Northern North Atlantic Ocean. *Glob. Planet. Chang.* **2013**, *111*, 199–225. [[CrossRef](#)]
50. Hickey, B.M.; Banas, N.S. Oceanography of the U.S. Pacific Northwest Coastal Ocean and Estuaries with Application to Coastal Ecology. *Estuaries* **2003**, *26*, 1010–1031. [[CrossRef](#)]
51. Largier, J.L. Upwelling Bays: How Coastal Upwelling Controls Circulation, Habitat, and Productivity in Bays. *Annu. Rev. Mar. Sci.* **2020**, *12*, 415–447. [[CrossRef](#)] [[PubMed](#)]
52. García-Reyes, M.; Largier, J. Observations of Increased Wind-Driven Coastal Upwelling off Central California. *J. Geophys. Res. Oceans* **2010**, *115*, 1–8. [[CrossRef](#)]
53. García-Reyes, M.; Largier, J.L. Seasonality of Coastal Upwelling off Central and Northern California: New Insights, Including Temporal and Spatial Variability. *J. Geophys. Res. Oceans* **2012**, *117*, 1–17. [[CrossRef](#)]
54. Arp, A.J.; Hansen, B.M.; Julian, D. Burrow Environment and Coelomic Fluid Characteristics of the Echiuran Worm Urechis Caupo from Populations at Three Sites in Northern California. *Mar. Biol.* **1992**, *113*, 613–623. [[CrossRef](#)]
55. Ricart, A.M.; Ward, M.; Hill, T.M.; Sanford, E.; Kroeker, K.J.; Takeshita, Y.; Merolla, S.; Shukla, P.; Ninokawa, A.T.; Elsmore, K.; et al. Coast-Wide Evidence of Low pH Amelioration by Seagrass Ecosystems. *Glob. Chang. Biol.* **2021**, *27*, 2580–2591. [[CrossRef](#)]
56. Silbiger, N.J.; Sorte, C.J.B. Biophysical Feedbacks Mediate Carbonate Chemistry in Coastal Ecosystems across Spatiotemporal Gradients. *Sci. Rep.* **2018**, *8*, 796. [[CrossRef](#)] [[PubMed](#)]
57. Kindeberg, T.; Bates, N.R.; Courtney, T.A.; Cyronak, T.; Griffin, A.; Mackenzie, F.T.; Paulsen, M.-L.; Andersson, A.J. Porewater Carbonate Chemistry Dynamics in a Temperate and a Subtropical Seagrass System. *Aquat. Geochem.* **2020**, *26*, 375–399. [[CrossRef](#)]
58. Schindelin, J.; Arganda-Carreras, I.; Frise, E.; Kaynig, V.; Longair, M.; Pietzsch, T.; Preibisch, S.; Rueden, C.; Saalfeld, S.; Schmid, B.; et al. Fiji: An Open-Source Platform for Biological-Image Analysis. *Nat. Methods* **2012**, *9*, 676–682. [[CrossRef](#)]
59. Brosset, C.; Höche, N.; Shirai, K.; Nishida, K.; Mertz-Kraus, R.; Schöne, B.R. Strong Coupling between Biomineral Morphology and Sr/Ca of Arctica Islandica (Bivalvia)—Implications for Shell Sr/Ca-Based Temperature Estimates. *Minerals* **2022**, *12*, 500. [[CrossRef](#)]
60. Schöne, B.R.; Radermacher, P.; Zhang, Z.; Jacob, D.E. Crystal Fabrics and Element Impurities (Sr/Ca, Mg/Ca, and Ba/Ca) in Shells of Arctica Islandica—Implications for Paleoclimate Reconstructions. *Palaeogeogr. Palaeoclimatol. Palaeoecol.* **2013**, *373*, 50–59. [[CrossRef](#)]
61. Arias, J.L.; Fernández, M.S. Polysaccharides and Proteoglycans in Calcium Carbonate-Based Biomineralization. *Chem. Rev.* **2008**, *108*, 4475–4482. [[CrossRef](#)]
62. Dauphin, Y.; Cuif, J.-P.; Doucet, J.; Salomé, M.; Susini, J.; Terry Willams, C. In Situ Chemical Speciation of Sulfur in Calcitic Biominerals and the Simple Prism Concept. *J. Struct. Biol.* **2003**, *142*, 272–280. [[CrossRef](#)]
63. Dauphin, Y.; Cuif, J.; Doucet, J.; Salomé, M.; Susini, J.; Williams, C. In Situ Mapping of Growth Lines in the Calcitic Prismatic Layers of Mollusc Shells Using X-ray Absorption near-Edge Structure (XANES) Spectroscopy at the Sulphur K-Edge. *Mar. Biol.* **2003**, *142*, 299–304. [[CrossRef](#)]
64. Guzman, N.; Ball, A.D.; Cuif, J.-P.; Dauphin, Y.; Denis, A.; Ortlieb, L. Subdaily Growth Patterns and Organo-Mineral Nanostructure of the Growth Layers in the Calcitic Prisms of the Shell of Concholepas Concholepas Bruguière, 1789 (Gastropoda, Muricidae). *Microsc. Microanal. Off. J. Microsc. Soc. Am. Microbeam Anal. Soc. Microsc. Soc. Can.* **2007**, *13*, 397–403. [[CrossRef](#)]
65. Addadi, L.; Raz, S.; Weiner, S. Taking Advantage of Disorder: Amorphous Calcium Carbonate and Its Roles in Biomineralization. *ChemInform* **2003**, *34*, 959–970. [[CrossRef](#)]
66. Ren, D.; Feng, Q.; Bourrat, X. Effects of Additives and Templates on Calcium Carbonate Mineralization in Vitro. *Micron* **2011**, *42*, 228–245. [[CrossRef](#)]
67. Dong, W.; Huang, J.; Liu, C.; Wang, H.; Zhang, G.; Xie, L.; Zhang, R. Characterization of the Myostracum Layers in Molluscs Reveals a Conservative Shell Structure. *Front. Mar. Sci.* **2022**, *9*, 544. [[CrossRef](#)]
68. Dicko, H.; Grünewald, T.A.; Ferrand, P.; Vidal-Dupiol, J.; Teaniniuraitemoana, V.; Koua, M.S.; le Moullac, G.; Le Luyer, J.; Saulnier, D.; Chamard, V.; et al. Sub-Micrometric Spatial Distribution of Amorphous and Crystalline Carbonates in Biogenic Crystals Using Coherent Raman Microscopy. *J. Struct. Biol.* **2022**, *214*, 107909. [[CrossRef](#)]
69. Duboisset, J.; Ferrand, P.; Baroni, A.; Grünewald, T.A.; Dicko, H.; Grauby, O.; Vidal-Dupiol, J.; Saulnier, D.; Gilles, L.M.; Rosenthal, M.; et al. Amorphous-to-Crystal Transition in the Layer-by-Layer Growth of Bivalve Shell Prisms. *Acta Biomater.* **2022**, *142*, 194–207. [[CrossRef](#)]
70. Grünewald, T.A.; Checchia, S.; Dicko, H.; Le Moullac, G.; Sham Koua, M.; Vidal-Dupiol, J.; Duboisset, J.; Nouet, J.; Grauby, O.; Di Michiel, M.; et al. Structure of an Amorphous Calcium Carbonate Phase Involved in the Formation of Pinctada Margaritifera Shells. *Proc. Natl. Acad. Sci. USA* **2022**, *119*, e2212616119. [[CrossRef](#)] [[PubMed](#)]

71. Taylor, M.; Simkiss, K.; Greaves, G.N. Amorphous Structure of Intracellular Mineral Granules. *Biochem. Soc. Trans.* **1986**, *14*, 549–552. [[CrossRef](#)] [[PubMed](#)]
72. Blue, C.R.; Dove, P.M. Chemical Controls on the Magnesium Content of Amorphous Calcium Carbonate. *Geochim. Cosmochim. Acta* **2015**, *148*, 23–33. [[CrossRef](#)]
73. Mancuso, A.; Stagoni, M.; Prada, F.; Scarponi, D.; Piccinetti, C.; Goffredo, S. Environmental Influence on Calcification of the Bivalve Chamelea Gallina along a Latitudinal Gradient in the Adriatic Sea. *Sci. Rep.* **2019**, *9*, 11198. [[CrossRef](#)] [[PubMed](#)]
74. Suzuki, M.; Nagasawa, H. Mollusk Shell Structures and Their Formation Mechanism. *Can. J. Zool.* **2013**, *91*, 349–366. [[CrossRef](#)]
75. Moss, D.K.; Ivany, L.C.; Jones, D.S. Fossil Bivalves and the Sclerochronological Reawakening. *Paleobiology* **2021**, *47*, 551–573. [[CrossRef](#)]
76. Hallmann, N.; Burchell, M.; Schöne, B.R.; Irvine, G.V.; Maxwell, D. High-Resolution Sclerochronological Analysis of the Bivalve Mollusk Saxidomus Gigantea from Alaska and British Columbia: Techniques for Revealing Environmental Archives and Archaeological Seasonality. *J. Archaeol. Sci.* **2009**, *36*, 2353–2364. [[CrossRef](#)]
77. Louis, V.; Besseau, L.; Lartaud, F. Step in Time: Biomineralisation of Bivalve's Shell. *Front. Mar. Sci.* **2022**, *9*, 1–16. [[CrossRef](#)]
78. Lutz, R.; Rhoads, D.C. Anaerobiosis and a Theory of Growth Line Formation. Available online: <https://www.science.org/doi/10.1126/science.198.4323.1222> (accessed on 21 February 2023).
79. Crenshaw, M.A. The Inorganic Composition of Molluscan Extrapallial Fluid. *Biol. Bull.* **1972**, *143*, 506–512. [[CrossRef](#)] [[PubMed](#)]
80. Littlewood, D.T.J.; Young, R.E. The Effect of Air-Gaping Behaviour on Extrapallial Fluid pH in the Tropical Oyster Crassostrea Rhizophorae. *Comp. Biochem. Physiol. A Physiol.* **1994**, *107*, 1–6. [[CrossRef](#)]
81. Clark, G.R. Daily Growth Lines in Some Living Pectens (Mollusca: Bivalvia), and Some Applications in a Fossil Relative: Time and Tide Will Tell. *Palaeogeogr. Palaeoclimatol. Palaeoecol.* **2005**, *228*, 26–42. [[CrossRef](#)]
82. Rodríguez-Tovar, F.J. Orbital Climate Cycles in the Fossil Record: From Semidiurnal to Million-Year Biotic Responses. *Annu. Rev. Earth Planet. Sci.* **2014**, *42*, 69–102. [[CrossRef](#)]
83. Richardson, C.A.; Crisp, D.J.; Runham, N.W. An Endogenous Rhythm in Shell Deposition in Cerastoderma Edule. *J. Mar. Biol. Assoc. U. K.* **1980**, *60*, 991–1004. [[CrossRef](#)]
84. Poulain, C.; Lorrain, A.; Flye-Sainte-Marie, J.; Amice, E.; Morize, E.; Paulet, Y.-M. An Environmentally Induced Tidal Periodicity of Microgrowth Increment Formation in Subtidal Populations of the Clam Ruditapes Philippinarum. *J. Exp. Mar. Biol. Ecol.* **2011**, *397*, 58–64. [[CrossRef](#)]
85. Richardson, C.A. Exogenous and Endogenous Rhythms of Band Formation in the Shell of the Clam Tapes Philippinarum (Adams et Reeve, 1850). *J. Exp. Mar. Biol. Ecol.* **1988**, *122*, 105–126. [[CrossRef](#)]
86. Chapman, E.C.; Bonsor, B.J.; Parsons, D.R.; Rotchell, J.M. Influence of Light and Temperature Cycles on the Expression of Circadian Clock Genes in the Mussel Mytilus Edulis. *Mar. Environ. Res.* **2020**, *159*, 104960. [[CrossRef](#)]
87. Ditty, J.L.; Williams, S.B.; Golden, S.S. A Cyanobacterial Circadian Timing Mechanism. *Annu. Rev. Genet.* **2003**, *37*, 513–543. [[CrossRef](#)]
88. Partch, C.L.; Green, C.B.; Takahashi, J.S. Molecular Architecture of the Mammalian Circadian Clock. *Trends Cell Biol.* **2014**, *24*, 90–99. [[CrossRef](#)]
89. Tan, Y.; Mero, M.; Roenneberg, T. Photoperiodism in Neurospora Crassa. *J. Biol. Rhythms* **2004**, *19*, 135–143. [[CrossRef](#)]
90. Comeau, L.A.; Babarro, J.M.F.; Longa, A.; Padin, X.A. Valve-Gaping Behavior of Raft-Cultivated Mussels in the Ría de Arousa, Spain. *Aquac. Rep.* **2018**, *9*, 68–73. [[CrossRef](#)]
91. Tran, D.; Perrigault, M.; Ciret, P.; Payton, L. Bivalve Mollusc Circadian Clock Genes Can Run at Tidal Frequency. *Proc. R. Soc. B* **2020**, *287*, 20192440. [[CrossRef](#)]
92. Aschoff, J. Freerunning and Entrained Circadian Rhythms. In *Biological Rhythms*; Aschoff, J., Ed.; Springer: Boston, MA, USA, 1981; pp. 81–93. [[CrossRef](#)]
93. Dunlap, J.C. Molecular Bases for Circadian Clocks. *Cell* **1999**, *96*, 271–290. [[CrossRef](#)] [[PubMed](#)]
94. Connor, K.M.; Gracey, A.Y. Circadian Cycles Are the Dominant Transcriptional Rhythm in the Intertidal Mussel Mytilus Californianus. *Proc. Natl. Acad. Sci. USA* **2011**, *108*, 16110–16115. [[CrossRef](#)] [[PubMed](#)]
95. Perrigault, M.; Tran, D. Identification of the Molecular Clockwork of the Oyster Crassostrea Gigas. *PLoS ONE* **2017**, *12*, e0169790. [[CrossRef](#)]
96. Pairett, A.N.; Serb, J.M. De Novo Assembly and Characterization of Two Transcriptomes Reveal Multiple Light-Mediated Functions in the Scallop Eye (Bivalvia: Pectinidae). *PLoS ONE* **2013**, *8*, e69852. [[CrossRef](#)] [[PubMed](#)]
97. Perrigault, M.; Andrade, H.; Bellec, L.; Ballantine, C.; Camus, L.; Tran, D. Rhythms during the Polar Night: Evidence of Clock-Gene Oscillations in the Arctic Scallop Chlamys Islandica. *Proc. R. Soc. B* **2020**, *287*, 20201001. [[CrossRef](#)] [[PubMed](#)]
98. Surge, D.; Lohmann, K.C.; Dettman, D.L. Controls on Isotopic Chemistry of the American Oyster, Crassostrea Virginica: Implications for Growth Patterns. *Palaeogeogr. Palaeoclimatol. Palaeoecol.* **2001**, *172*, 283–296. [[CrossRef](#)]
99. Tynan, S.; Dutton, A.; Eggins, S.; Opdyke, B. Oxygen Isotope Records of the Australian Flat Oyster (Ostrea Angasi) as a Potential Temperature Archive. *Mar. Geol.* **2014**, *357*, 195–209. [[CrossRef](#)]
100. Owen, R.; Kennedy, H.; Richardson, C. Isotopic Partitioning between Scallop Shell Calcite and Seawater: Effect of Shell Growth Rate. *Geochim. Cosmochim. Acta* **2002**, *66*, 1727–1737. [[CrossRef](#)]
101. Huyghe, D.; de Rafelis, M.; Ropert, M.; Mouchi, V.; Emmanuel, L.; Renard, M.; Lartaud, F. New Insights into Oyster High-Resolution Hinge Growth Patterns. *Mar. Biol.* **2019**, *166*, 48. [[CrossRef](#)]

102. Trofimova, T.; Alexandroff, S.J.; Mette, M.J.; Tray, E.; Butler, P.G.; Campana, S.E.; Harper, E.M.; Johnson, A.L.A.; Morrongiello, J.R.; Peharda, M.; et al. Fundamental Questions and Applications of Sclerochronology: Community-Defined Research Priorities. *Estuar. Coast. Shelf Sci.* **2020**, *245*, 106977. [[CrossRef](#)]
103. Jones, D.S. Annual Cycle of Shell Growth Increment Formation in Two Continental Shelf Bivalves and Its Paleocologic Significance. *Paleobiology* **1980**, *6*, 331–340. [[CrossRef](#)]
104. Epstein, S.; Buchsbaum, R.; Lowenstam, H.A.; Urey, H.C. Revised carbonate-water isotopic temperature scale. *GSA Bull.* **1953**, *64*, 1315–1326. [[CrossRef](#)]
105. Jones, D.S.; Quitmyer, I.R. Marking Time with Bivalve Shells; Oxygen Isotopes and Season of Annual Increment Formation. *Palaios* **1996**, *11*, 340–346. [[CrossRef](#)]
106. Burchell, M.; Cannon, A.; Hallmann, N.; Schwarcz, H.P.; Schöne, B.R. Refining Estimates for the Season of Shellfish Collection on the Pacific Northwest Coast: Applying High-Resolution Stable Oxygen Isotope Analysis and Sclerochronology. *Archaeometry* **2013**, *55*, 258–276. [[CrossRef](#)]
107. Chute, A.S.; Wainright, S.C.; Hart, D.R. Timing of Shell Ring Formation and Patterns of Shell Growth in the Sea Scallop *Placopecten Magellanicus* Based on Stable Oxygen Isotopes. *J. Shellfish Res.* **2012**, *31*, 649–662. [[CrossRef](#)]
108. Kennedy, H.; Richardson, C.; Duarte, C.; Kennedy, D. Oxygen and Carbon Stable Isotopic Profiles of the Fan Mussel, *Pinna Nobilis*, and Reconstruction of Sea Surface Temperatures in the Mediterranean. *Mar. Biol.* **2001**, *139*, 1115–1124. [[CrossRef](#)]
109. Klein, R.T.; Lohmann, K.C.; Thayer, C.W. Bivalve Skeletons Record Sea-Surface Temperature and $\delta^{18}\text{O}$ via Mg/Ca and $^{18}\text{O}/^{16}\text{O}$ Ratios. *Geology* **1996**, *24*, 415–418. [[CrossRef](#)]
110. Krantz, D.E.; Jones, D.S.; Williams, D.F. Growth Rates of the Sea Scallop, *Placopecten Magellanicus*, Determined from the $^{18}\text{O}/^{16}\text{O}$ Record in Shell Calcite. *Biol. Bull.* **1984**, *167*, 186–199. [[CrossRef](#)]
111. Tan, F.C.; Cai, D.; Roddick, D.L. Oxygen Isotope Studies on Sea Scallops, *Placopecten Magellanicus*, from Browns Bank, Nova Scotia. *Can. J. Fish. Aquat. Sci.* **1988**, *45*, 1378–1386. [[CrossRef](#)]
112. Balestra, B.; Rose, T.; Fehrenbacher, J.; Knobelspiesse, K.D.; Huber, B.T.; Gooding, T.; Paytan, A. In Situ Mg/Ca Measurements on Foraminifera: Comparison between Laser Ablation Inductively Coupled Plasma Mass Spectrometry and Wavelength-Dispersive X-ray Spectroscopy by Electron Probe Microanalyzer. *Geochem. Geophys. Geosyst.* **2021**, *22*, e2020GC009449. [[CrossRef](#)]
113. Poitevin, P.; Chauvaud, L.; Pécheyran, C.; Lazure, P.; Jolivet, A.; Thébault, J. Does Trace Element Composition of Bivalve Shells Record Ultra-High Frequency Environmental Variations? *Mar. Environ. Res.* **2020**, *158*, 104943. [[CrossRef](#)]
114. Soldati, A.L.; Jacob, D.E.; Schöne, B.R.; Bianchi, M.M.; Hajduk, A. Seasonal Periodicity of Growth and Composition in Valves of *Diplodon Chilensis Patagonicus* (d’Orbigny, 1835). *J. Molluscan Stud.* **2009**, *75*, 75–85. [[CrossRef](#)]

Disclaimer/Publisher’s Note: The statements, opinions and data contained in all publications are solely those of the individual author(s) and contributor(s) and not of MDPI and/or the editor(s). MDPI and/or the editor(s) disclaim responsibility for any injury to people or property resulting from any ideas, methods, instructions or products referred to in the content.